Title

Timing and mechanism for intratest Mg/Ca variability in a living planktic foraminifer

Authors

Spero, Howard J
Eggins, Stephen M
Russell, Ann D
et al.

Publication Date

2015

DOI

10.1016/j.epsl.2014.10.030

Peer reviewed

Earth and Planetary Science Letters 409 (2015) 32–42

Contents lists available at ScienceDirect

Earth and Planetary Science Letters

www.elsevier.com/locate/epsl

Timing and mechanism for intratest Mg/Ca variability in a living planktic foraminifer

Howard J. Spero [a,*], Stephen M. Eggins [b], Ann D. Russell [a], Lael Vetter [a,1], Matt R. Kilburn [c], Bärbel Hönisch [d]

[a] Department of Earth and Planetary Sciences, University of California Davis, Davis, CA 95616, USA
[b] Research School of Earth Sciences, The Australian National University, Canberra, ACT 0200, Australia
[c] Center for Microscopy, Characterisation and Analysis, University of Western Australia, Crawley, WA 6009, Australia
[d] Department of Earth and Environmental Sciences and Lamont-Doherty Earth Observatory of Columbia University, 61 Route 9W, Palisades, NY 10964, USA

ARTICLE INFO

Article history:
Received 2 April 2014
Received in revised form 28 September 2014
Accepted 18 October 2014
Available online xxxx
Editor: J. Lynch-Stieglitz

Keywords:
foraminifera Mg/Ca
Mg banding
laser ablation ICP-MS
Orbulina universa
paleothermometer
mitochondria

ABSTRACT

Geochemical observations indicate that planktic foraminifer test Mg/Ca is heterogeneous in many species, thereby challenging its use as a paleotemperature proxy for paleoceanographic reconstructions. We present Mg/Ca and Ba/Ca data collected by laser ablation ICP-MS from the shells of *Orbulina universa* cultured in controlled laboratory experiments. Test calcite was labeled with Ba-spiked seawater for 12 h day or night calcification periods to quantify the timing of intratest Mg-banding across multiple diurnal cycles. Results demonstrate that high Mg bands are precipitated during the night whereas low Mg bands are precipitated during the day. Data obtained from specimens growing at 20 °C and 25 °C show that Mg/Ca ratios in both high and low Mg bands increase with temperature, and average test Mg/Ca ratios are in excellent agreement with previously published empirical calibrations based on bulk solution ICP-MS analyses. In general, Mg band concentrations decrease with increasing pH and/or $[CO_3^{2-}]$ but this effect decreases as experimental temperatures increase from 20 °C to 25 °C. We suggest that mitochondrial uptake of Mg^{2+} from the thin calcifying fluid beneath streaming rhizopodial filaments may provide the primary locus for Mg^{2+} removal during test calcification, and that diurnal variations in either mitochondrial density or activity produce Mg banding. These results demonstrate that Mg banding is an inherent component of test biomineralization in *O. universa* and show that the Mg/Ca paleothermometer remains a fundamental tool for reconstructing past ocean temperatures from fossil foraminifers.

1. Introduction

Laboratory (Lea et al., 1999; Nürnberg et al., 1996), core-top (Dekens et al., 2002; Elderfield and Ganssen, 2000; Rosenthal and Lohmann, 2002) and sediment trap (Anand et al., 2003; McConnell and Thunell, 2005) studies have established Mg/Ca paleothermometry as a key paleoceanographic tool for reconstructing past ocean temperatures from fossil planktic and benthic foraminifers. Other environmental factors, such as seawater pH or $[CO_3^{2-}]$ (Lea et al., 1999; Russell et al., 2004; Yu and Elderfield, 2008) and possibly salinity (Arbuszewski et al., 2010; Kisakürek et al., 2008; Mathien-Blard and Bassinot, 2009), can influence test Mg/Ca, but these effects are minor relative to the overwhelming control of temperature on test Mg (Hönisch et al., 2013; Lea et al., 1999; Russell et al., 2004).

Studies with the electron microprobe (Brown and Elderfield, 1996; Eggins et al., 2004; Erez, 2003; Fehrenbacher and Martin, 2014; Hathorne et al., 2009; Sadekov et al., 2005; Toyofuku and Kitazato, 2005), laser ablation inductively coupled plasma mass spectrometry (LA-ICP-MS), and NanoSIMS technologies (Eggins et al., 2003; Hathorne et al., 2003; Kunioka et al., 2006) have demonstrated large intratest Mg/Ca variability and banding patterns in many species of planktic foraminifers. These observations have added a level of complexity to the interpretation of Mg/Ca as a high-precision proxy for paleoceanographic applications (Eggins et al., 2004; Sadekov et al., 2005).

Researchers agree that temperature variation due to depth migration during the 2–4 week life cycle of a planktic foraminifer cannot account for intratest Mg/Ca variation in tests collected from sediment traps or core tops because the implied temperature range of 10 to 15 °C is unrealistic for the water column hydrography at

* Corresponding author. Tel.: +1 530 752 3307.
E-mail address: hjspero@ucdavis.edu (H.J. Spero).
[1] Current address: Department of Earth and Environmental Sciences, Tulane University, New Orleans, LA 70118, USA.

http://dx.doi.org/10.1016/j.epsl.2014.10.030
0012-821X/

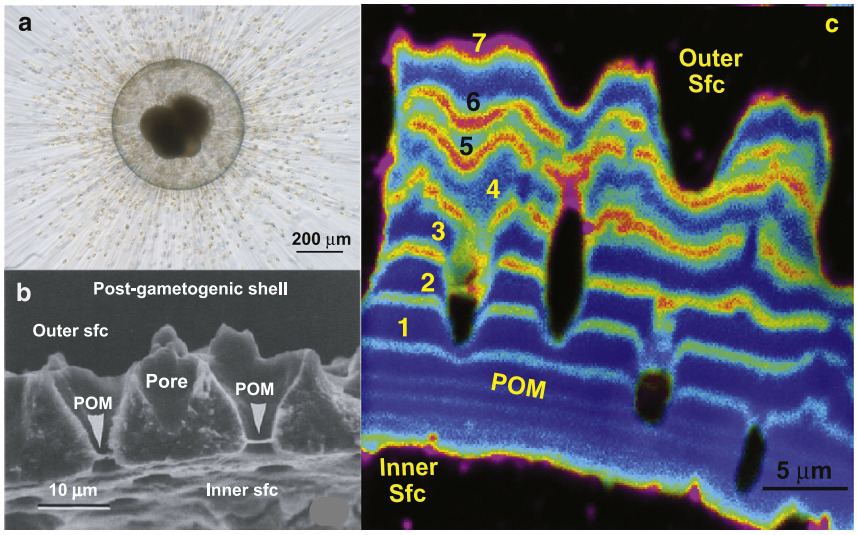

Fig. 1. (a) Living *Orbulina universa* with recently precipitated spherical chamber (~4 h old) surrounding a juvenile trochospiral shell that contains foraminifer cytoplasm. Sphere thickness is estimated to be <0.5 µm at this stage of calcification, with a sphere diameter of 464 µm. (b) SEM cross-section through a spherical chamber after gametogenesis in the laboratory. Primary organic membrane (POM) is evident near the inner surface of the chamber as are deeply incised pores. Image modified from Spero (1988). (c) NanoSIMS image of a post-gametogenic *O. universa* sphere cross-section (AMMRF Profile Report, 2008). Seven high (bright bands) and low (dark bands) Mg banding pairs can be identified on the outer surface of the POM, reflecting 7 days of growth in the laboratory. Closely spaced Mg bands can be seen on the inner side of the POM. Note that both the low and high Mg bands near the outer test surface contain elevated Mg relative to earlier bands near the POM. Voids in the image are oblique cuts through pores in (b).

collection sites (Anand and Elderfield, 2005; Eggins et al., 2004; Hathorne et al., 2009). Eggins et al. (2004) proposed instead that the Mg/Ca banding might be diurnal and linked to symbiont photosynthesis, respiration, or some other physiological process that affects microenvironmental carbonate chemistry at the site of calcification across a diel cycle. Such a mechanism could explain Mg/Ca heterogeneity observed in symbiotic species (Gastrich, 1987) such as *O. universa*, *Globigerinoides ruber* (Sadekov et al., 2008), *G. sacculifer* (Sadekov et al., 2009), *Neogloboquadrina dutertrei* (Fehrenbacher and Martin, 2010), *Globorotalia inflata* (Hathorne et al., 2009) and *Pulleniatina obliquiloculata* (Kunioka et al., 2006; Sadekov et al., 2009), but cannot account for similar Mg/Ca patterns in non-symbiotic species such as *Globorotalia truncatulinoides* (McKenna and Prell, 2004), *G. scitula* (Hathorne et al., 2009) or *Globigerina bulloides* (Anand and Elderfield, 2005). Modeling results also show that Rayleigh fractionation in the calcifying reservoir (Elderfield et al., 1996), and crystal structure changes (Davis et al., 2004) are unable to explain observed intratest Mg/Ca and other elemental variations (Hathorne et al., 2009).

In this study we present the results of laboratory experiments with the planktic foraminifer species *O. universa* that constrain the timing of high and low Mg band deposition during calcification and provide evidence for a physiological mechanism for Mg/Ca variability that could apply to both symbiotic and non-symbiotic foraminifers. We use *O. universa* because it produces a spherical chamber of calcite (Fig. 1a) that thickens continuously during the last ~2–9 days of its life cycle (Fig. 1b) (Spero, 1988) and displays a reproducible Mg banding pattern throughout its test (Eggins et al., 2004) (Fig. 1c). Previous experiments with *O. universa* have quantified the relationship between test Mg/Ca and temperature, pH ($[CO_3^{2-}]$), and symbiont photosynthesis (Lea et al., 1999; Russell et al., 2004), and have also demonstrated that Ba^{2+} is incorporated into test calcite in proportion to seawater concentration, irrespective of these environmental and biological parameters (Hönisch et al., 2011; Lea and Spero, 1992, 1994). Here, we explore intratest variability in Mg^{2+} by labeling calcite precipitated during defined periods of test growth with dissolved barium.

2. Materials and methods

2.1. Foraminifer collection and maintenance

In July–August 2007, pre-sphere, trochospiral test stage *O. universa* (250–350 µm test length) were hand-collected by scuba divers from a depth of 2–6 m in the San Pedro Basin, Southern California Bight (33°23′N, 118°26′W). Freshly collected specimens were transported from the collection site to the Wrigley Marine Science Center of the University of Southern California on Santa Catalina Island (~2 km distance) where they were identified, measured, and transferred into 120 mL soda lime glass jars (Wheaton©) containing 0.8 µm filtered seawater. Snap lids, lined with Parafilm M laboratory film, were used to seal the jars without an air space to maintain stable carbonate chemistry. The jars were then placed into water tanks which were maintained at temperatures of 20 or 25 °C (±0.2 °C). Illumination was provided by F24T12/CW/HO fluorescent bulbs on a 12:12 h light:dark cycle. All specimens were maintained under sufficiently high light levels (>300 µmol photons m^{-2} s^{-1}, PAR) to maximize symbiont photosynthetic rates (Rink et al., 1998; Spero and Parker, 1985). Each foraminifer was fed a one-day-old *Artemia* nauplius every third day until gametogenesis (Bé et al., 1983), which typically occurred 6–10 days after collection.

2.2. Water chemistry modification experiments

Temperature, salinity, and carbonate system parameters are given in Table 1. Total alkalinity was determined by Gran-titration with a Metrohm 785 Titrino autotitrator, and was standardized using Dickson certified alkalinity reference material. pH_{NBS} was measured with the Metrohm pH electrode after calibrating with low-ionic strength Fisher buffers. Seawater alkalinity was increased for the $[CO_3^{2-}]$ experiments by adding 0.1 N NaOH. Average $[CO_3^{2-}]$ compositions were computed from initial seawater and randomly selected samples at the end of each experiment, using the program CO2calc (Robbins et al., 2010). Measured and calculated parameters are given in Table 1. In further discussion, we refer to the calculated pH_{sws} (rather than the measured pH_{NBS}) to conform with

Table 1
Water carbonate chemistry.

	Measured parameters				Calculated parameters		
	T (°C)	S	Total alkalinity ($\mu eq\,kg^{-1}$)	pH_{NBS}	DIC ($\mu mol\,kg^{-1}$)[a]	$[CO_3^{2-}]$ ($\mu mol\,kg^{-1}$)[a]	pH_{sws}[b]
Ambient seawater	21 ± 0.6	34	2263 ± 10	8.16 ± 0.03	2019 ± 10	177 ± 1	8.01
Low-T, high-$[CO_3^{2-}]$	20	34	2498 ± 9	8.44 ± 0.03	2069 ± 24	307 ± 14	8.29
High-T, high-$[CO_3^{2-}]$	25	34	2498 ± 9	8.38 ± 0.03	2066 ± 24	308 ± 18	8.22

[a] Calculated from pH_{NBS} and total alkalinity using CO2calc (Robbins et al., 2010), with K1, K2 from Mehrbach et al. (1973), $KHSO_4$ from Dickson (1990), and the option for pH on the NBS scale.

[b] Calculated from dissolved inorganic carbon (DIC) and total alkalinity using CO2calc, with K1, K2 from Mehrbach et al. (1973) (as refit by Dickson and Millero (1987) to the seawater pH scale), $KHSO_4$ from Dickson (1990), and the option for pH on the seawater scale.

current practice, but keep pH_{NBS} in Table 1 to facilitate comparisons with our previous work.

Ba spike preparation followed the procedure of Lea and Spero (1992). Ba-spiked water for the foraminifers was prepared by adding a solution of $BaCl_2$ in deionized water to filtered seawater (ambient $[Ba]_{sw} = 38\ nmol\,kg^{-1}$) to produce a final $[Ba]_{sw}$ of ~200 $nmol\,kg^{-1}$. This concentration is below the saturation limit of barite ($BaSO_4$) in seawater and is ~5× ambient seawater concentrations (Church and Wolgemuth, 1972). In all cases, addition of the Ba solution had a negligible effect on the Cl^- content or pH of the culture water. During the experiments, water displaced during feeding was replaced with filtered seawater of the same chemical composition.

For the 12:12 h light:dark cycle Ba-labeling and pH experiments, trochospiral test *O. universa* were grown in ambient seawater through sphere formation. Specimens were then kept in ambient seawater for 12 h during the day (07:00 to 19:00 h), and transferred to seawater in which the dissolved $[Ba]_{sw}$ was increased from ambient concentrations of 38 $nmol\,kg^{-1}$ to ~200 $nmol\,kg^{-1}$ during the 12 h dark period, or vice versa (see Vetter et al., 2013 for additional details). This 12 h transfer cycle was repeated between ambient and Ba-spiked seawater until the foraminifers underwent gametogenesis. Empty tests were then rinsed in ≥18.2 MΩ deionized water and archived in multihole storage slides for later analysis.

2.3. Sample preparation and cleaning for LA-ICP-MS

Individual tests were cracked and split into 2–3 fragments using the point of a scalpel blade. Fragments were then cleaned by ultrasonicating in methanol, followed by a triple rinse in distilled water and oxidative cleaning at 60 °C for 30 min in a buffered hydrogen peroxide solution (1:1 mix of saturated H_2O_2 solution and 0.1 M NaOH) (Pak et al., 2004), and finally a triple rinse in distilled water. Single fragments from each test were attached to black, double-sided, carbon-conductive tape on a standard glass microscope slide with the inner test surface facing upwards. This positioning supports the fragile test wall during laser ablation analysis and permits the determination of a complete compositional profile through the full thickness of the chamber wall (Eggins et al., 2004).

2.4. Laser ablation ICP-MS analysis

A LA-ICP-MS technique that achieves sub-micron depth resolution was employed to profile variations in Mg, Ca, and Ba from the inner to the outer surface of the mounted test fragments. Samples were analyzed in an ANU-designed Helex dual-volume laser ablation cell at the Australian National University using an ArF excimer laser coupled to an Agilent 7500s quadrupole ICP-MS (Eggins et al., 2003, 2004). In brief, precise depth profiling of foraminifer test walls is accomplished by using a deep UV laser wavelength (λ = 193 nm, 25 ns pulse width) and simple mask projection optics to deliver a modest uniform laser fluence (4 $J\,cm^{-2}$) to the sample target such that each laser pulse ablates a ~0.1 μm thick layer from the test surface.

Laser sampling is conducted in a He atmosphere to maximize sample yield (Eggins et al., 1998). The ablation products are transported in a mixed He–Ar gas flow from the Helex ablation cell to the ICP-MS via a 10-path distributed delay manifold ('squid') that smooths laser pulse harmonics (Eggins et al., 1998). The resulting sample washout response is close to one order of magnitude per second such that depth resolution of the analysis is optimized by ablating at 4 laser pulses per second and by targeting test surfaces that are orthogonal to the laser beam. The depth resolution degrades as the ablation pit deepens due to an unavoidable increase in sample yield from the ablation pit walls (Eggins et al., 1998). Each test wall profile analysis consumes only about 10 ng of test material, or <0.1% of the total test mass, and typically takes between 20 and 60 s to complete.

A small number of isotopes and elements (typically ^{24}Mg, ^{25}Mg, ^{27}Al, ^{43}Ca, ^{44}Ca, ^{55}Mn, ^{88}Sr, ^{138}Ba) are measured simultaneously using a rapid peak hopping procedure as laser ablation proceeds through test walls. The ICP-MS is tuned for optimum sensitivity subject to maintaining $ThO^+/Th^+ < 0.5\%$. Between 100–250 data points per test wall profile are generated for each analyzed isotope, depending on test wall thickness. Multiple compositional profiles (2 or 3 per test) are determined from the mounted fragment of each test. The mean element/Ca ratio composition of each profile is then averaged to obtain an estimate of the bulk-test element/Ca ratio for each specimen (Suppl. Table 1).

Data reduction follows established protocols for time-resolved analysis (Longerich et al., 1996), and is undertaken on dead time-corrected raw count values extracted from the mass spectrometer as an $m \times n$ matrix of values for each isotope (m) measured in each mass spectrometer cycle (n). Drift-corrected background count rates, measured with the laser off immediately prior to bracketing NIST SRM610 glass calibration analyses, is subtracted from the raw counts. The background-corrected count rates are screened for outliers arising from particulates ejected from the sample by laser induced shockwaves. These outliers are identified based on signal intensity reductions that are more rapid than the characteristic signal washout response of the Helex ablation system (see Table 2). The resulting count rates are corrected for ablation yield by ratio to the weighted mean (ΣCa) of the corrected ^{43}Ca and ^{44}Ca count rates for each mass spectrometer cycle, and referenced to equivalent drift-corrected ratios in bracketing analyses of NIST SRM610 glass to calculate element/Ca molar ratios. The composition of the NIST610 glass is taken to be Mg = 465 $\mu g\,g^{-1}$, Al = 10,796 $\mu g\,g^{-1}$, Ca = 81,830 $\mu g\,g^{-1}$, Mn = 485 $\mu g\,g^{-1}$, Sr = 515.5 $\mu g\,g^{-1}$ (Pearce et al., 1997; Reed, 1992), and a preferred Ba = 450 $\mu g\,g^{-1}$, based on cross calibration with other silicate glass reference materials at the Australian National University (ANU). The reported Mg/Ca ratio is also the mean of values calculated from $^{24}Mg/\Sigma Ca$ and $^{25}Mg/\Sigma Ca$ values in each mass spectrometer cycle.

Table 2
ICP-MS and laser ablation operating conditions.

Agilent 7500s	Operated without shield torch
ICP forward power	1300 W
$^{232}Th^{16}O^+/^{232}Th^+$	<0.5%
Quadrupole sampling	1 point per peak
Isotope dwell times (ms)	30 ms (^{25}Mg, ^{43}Ca, ^{55}Mn, ^{88}Sr, ^{138}Ba), 20 ms (^{24}Mg, ^{44}Ca), 10 ms (^{27}Al)
Cycle time	0.286 s
ETP detector dead time	39.5 ns
ANU Helex laser ablation system	
Wavelength	193 nm
Laser fluence/power density	4 J cm^{-2}, 0.16 GW cm^{-2}
Laser pulse length	25 ns
Laser pulse repetition rate	4 Hz
He flow rate through bottom of dual volume cell	500 cm^3 min^{-1}
Ar flow rate through top of dual volume cell	1200 cm^3 min^{-1}
Projected laser ablation circular spot size	28 and 37 µm
Signal intensity decay (washout) $I = I_0 \exp^{(-t/\tau)}$ [a]	$\tau = 0.55$ s

[a] Where $t =$ time in seconds and τ is the particulate residence time in the cell.

2.5. NanoSIMS preparation and imaging

A pre-sphere specimen of *O. universa* was collected by plankton tow off the SE coast of Australia near Eden, New South Wales. The specimen was grown in the laboratory at ANU in a 22 ml glass vial at 22 °C and was fed a one-day-old *Artemia* nauplius daily until gametogenesis. Uncleaned fragments of the test were embedded in epoxy resin, and then polished with a series of diamond polishing powders (down to 1 µm) to minimize surface topography. The mount was coated with a 5 nm-layer of gold to provide conductivity at high voltage.

High-resolution elemental imaging was performed using the CAMECA NanoSIMS 50 at The University of Western Australia. The mass spectrometer was tuned to detect the positive secondary ions $^{24}Mg^+$, $^{40}Ca^+$, $^{55}Mn^+$, $^{88}Sr^+$, and $^{138}Ba^+$, sputtered from the sample surface using an O^- primary beam. Peak positions were calibrated using pure metals and NIST SRM610 standards. Prior to image acquisition, each region of interest was pre-sputtered using a high-density primary beam to achieve an ion dose of $>5 \times 10^{16}$ ions cm^{-2}. This removed any surface contaminants, implanted O^--ions into the sample matrix, and enabled an approximate steady state of ion emission to be reached. High-resolution images were acquired with a beam current of 25 pA, producing a spot size between 500 and 600 nm in diameter. The beam was scanned over an area 50 × 50 µm, at a pixel resolution of 256 × 256, with a dwell time of 30 ms pixel^{-1}. Ion images were processed using the Open-MIMS plugin (http://www.nrims.hms.harvard.edu/software.php) for ImageJ (http://rsbweb.nih.gov/ij/). Ratio images were obtained by dividing the Mg image by the Ca images using a ratio scale factor of 10.000.

3. Results

3.1. O. universa test calcification and NanoSIMS observations

The *O. universa* sphere is the final chamber produced during the species life cycle (Fig. 1a). Sphere thickening continues for the next ~2–9 days followed by gametogenesis. A cross-section through a post-gametogenic sphere displays deeply incised pores and the primary organic membrane (POM) that corresponds to the initial calcite deposited in the sphere (Fig. 1b). This image shows that most test thickening occurs between the POM and the outer sphere surface.

The NanoSIMS image is a cross-section through an *O. universa* sphere that was maintained in culture for a period of 7 days following sphere formation and displays 7 high and 7 low Mg/Ca ratio bands on the outer side of the POM (Fig. 1c). The number of Mg bands is consistent with the hypothesis of Eggins et al. (2004) that Mg banding is related to a daily cycle. In this image, pores are evident as oval voids in the Mg bands. The POM is a region of low Mg/Ca ratios that separates more widely spaced low and high Mg bands in the outer test from more closely spaced bands near the inner test surface (Fig. 1c). The high Mg bands in the outer test region are ~1–1.5 µm wide and separated by 2–3-µm-wide low Mg bands. In contrast, high and low Mg bands below the POM are closely spaced and have widths that range from ~300–800 nm. The NanoSIMS image also records a trend of increasing Mg towards inner and outer surfaces in both high and low Mg bands as test thickening progresses. The thin layers of high Mg on the inner and outer test surfaces could be due to residual organic matter, as this specimen was not cleaned with oxidants prior to embedding and polishing.

3.2. Ba labeling experiments

Fig. 2a shows a single depth profile ablated through the shell of an *O. universa* grown at 20 °C in ambient seawater on Santa Catalina Island (specimen #103a2). Four high and low Mg bands can be seen with increasing Mg/Ca as calcification proceeds from the low Mg POM region to the outer surface. These data are similar to the pattern seen in the NanoSIMS image (Fig. 1c). The Mg/Ca ratios in this profile range between 2.7 to 11.7 mmol mol^{-1} (Table 3), with an average Mg/Ca across the profile of 5.9 ± 0.4 mmol mol^{-1} ($n = 168$ mass spectrometer cycles; ±2 s.e.). Three to four thin high Mg bands are partially resolved in the portion of the calcite shell that is precipitated inside of the POM. The effective spatial resolution of the laser ablation depth profile increases from a few hundred nanometers to over 1 µm with increasing ablation depth, such that it is difficult to resolve the full amplitude of the outer high and low Mg bands (deepest region of the laser pit) that might otherwise be detected using NanoSIMS. These data also show that despite the oscillatory Mg/Ca banding, the intrashell Ba/Ca in *O. universa* is uniform across the chamber wall in the direction of growth, with an average Ba/Ca ratio for this profile of 0.69 ± 0.02 µmol mol^{-1} (±2 s.e.). Note that the standard errors of the mean Mg/Ca and Ba/Ca profiles provide 95% confidence estimates for the profile averages.

Multiple depth profiles ablated through sphere fragments of several specimens demonstrate the extent to which profiles can be reproduced, as well as the average elemental/Ca ratio homogeneity of *O. universa* tests (Table 3; Suppl. Fig. 1). Mean Mg/Ca and Ba/Ca ratios from seven laser ablation profiles in two test fragments of specimen #103 measured on two different days are 6.0 ± 0.2 mmol mol^{-1} and 0.60 ± 0.05 µmol mol^{-1}, respectively.

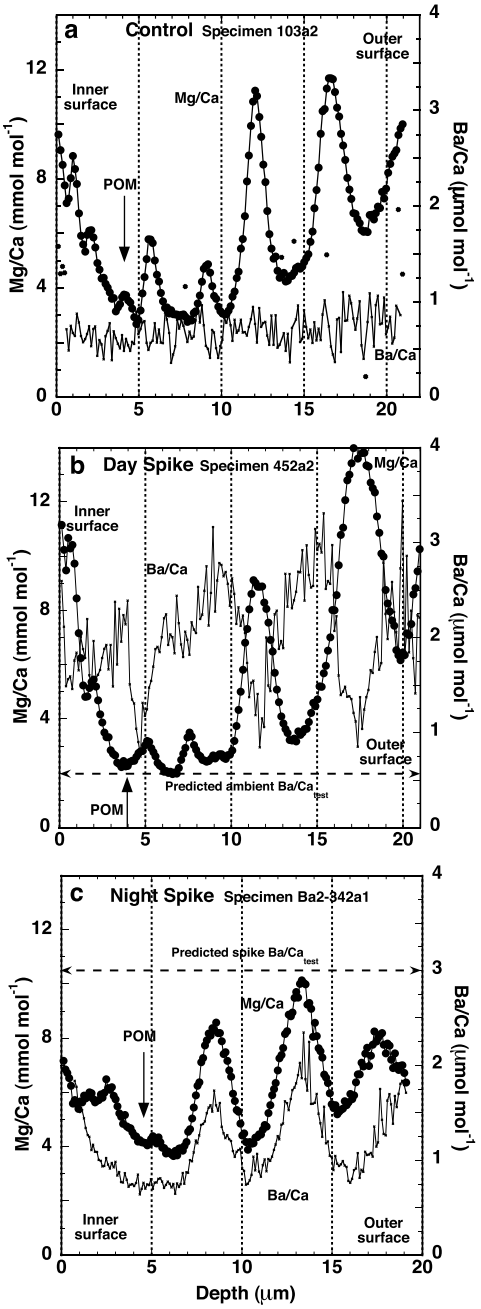

Fig. 2. LA-ICP-MS transects through post-gametogenic *O. universa* that were grown at 20 °C on a 12 h:12 h light:dark cycle. Mg/Ca (black dots) and Ba/Ca (thin line) ratios were collected from inner to outer test surfaces. (a) Control specimen #103a2 grown continuously in ambient seawater. Discrete black diamonds on plot are Ba/Ca data not included in the transect average (11/168 points) due to edge effects and random data spikes. See Suppl. Fig. 1 for replicate profiles through this specimen. (b) Specimen 452a2 grown in ambient seawater during the light phase and Ba-spiked seawater during the day phase. (c) Specimen Ba2-342a1 grown in Ba-spiked seawater during the dark phase and ambient seawater during the light phase. This specimen was collected in the field after its spherical chamber had been produced. The first Ba spike appears in the second high Mg band, indicating the sphere was 24 h old when collected.

We have obtained similar Mg/Ca reproducibility of mean test composition in specimens #342 (6.4 ± 0.2 mmol mol^{-1}) and #344 (Mg/Ca $= 6.6 \pm 0.1$ mmol mol^{-1}), which were each analyzed with six repeat depth profiles (Table 3; note comparative Ba/Ca averages are not meaningful for these 12 h Ba-spike specimens). Mean Ba/Ca for specimen #103 agrees closely with a predicted ratio of 0.55 µmol mol^{-1} (Hönisch et al., 2011; Lea and Spero, 1992) that is calculated from published empirical calibrations based on bulk analyses of many foraminifer tests grown in culture.

We conducted two tracer experiments to constrain the timing of high and low Mg band development in *O. universa*. Because Ba/Ca is uniform throughout the tests of *O. universa* maintained in ambient seawater (Fig. 2a), and [Ba] increases in shells in proportion to seawater [Ba], we are able to induce artificial intratest Ba/Ca oscillations by transferring the specimens in and out of Ba-spiked seawater either during the day or during the night. The resulting intratest Ba-labeled bands in the *O. universa* sphere demonstrate that the low Mg bands are precipitated during the daytime period and the high Mg bands are precipitated at night (Figs. 2b and 2c). The low Mg bands are approximately two to three times the width of the high Mg bands (measured at half their maximum height), which is broadly consistent with previous calculations of the amount of shell calcite added during day (66%) compared to night (33%) (Lea et al., 1995; Spero, 1988). However, Ba/Ca attains predicted ratios only during daytime calcification periods, indicating that the full Ba signal may not be fully resolved in thinner night-time bands (Vetter et al., 2013). Mean Mg/Ca ratios for the specimens in Figs. 2b and 2c are 5.7 ± 0.2 mmol mol^{-1} ($n = 2$; ± 2 s.e.) and 6.0 ± 0.2 mmol mol^{-1} ($n = 4$). Both averages are in excellent agreement with predicted bulk-test Mg/Ca ratios for 20 °C despite having different Mg/Ca amplitude ranges relative to the specimen in Fig. 2a (also see Suppl. Fig. 1 and Suppl. Table 1).

Data in Fig. 2 are also consistent with the NanoSIMS results (Fig. 1c), which show that the high Mg bands contain a central region of elevated Mg surrounded by shoulders with increasing and decreasing Mg. It is notable that the Ba/Ca ratio varies together with Mg/Ca across the high Mg bands. This likely reflects a loss of depth resolution and averaging across low and high Mg bands, rather than being a function of uptake differences between the Ba and Mg cations. Together, these data indicate that Mg/Ca banding in the *O. universa* test is related to a diurnal cycle in foraminifer physiology that is linked to light.

3.3. Carbonate ion experiments

We examine the influence of seawater pH and/or [CO_3^{2-}] on Mg/Ca banding with *O. universa* by comparing profile compositions grown at constant temperature (20 °C or 25 °C) in ambient seawater ($pH_{sws} = 8.01$, [CO_3^{2-}] $= 177$ µmol kg^{-1}) with those grown continuously or for 12 h day or night periods in seawater with elevated [CO_3^{2-}] (at 20 °C, $pH_{sws} = 8.29$ and [CO_3^{2-}] $= 307$ µmol kg^{-1}; at 25 °C, $pH_{sws} = 8.22$ and [CO_3^{2-}] $= 308$ µmol kg^{-1}) (Table 1). In general, the overall average Mg/Ca ratio decreases, peak amplitudes are lower, and the peak widths are broader in the high pH experiments, compared to specimens grown continuously in ambient seawater (Fig. 3). For tests grown at 20 °C, the Mg/Ca decrease is 28%, which is significant at $p < 0.01$ (student's t test), whereas the 9% Mg/Ca decrease in the 25 °C group is not significant at $p < 0.05$ (Fig. 4a).

We also compare the Mg/Ca compositions of *O. universa* grown in ambient seawater with those grown in elevated pH during the 12 h night or day periods in an effort to isolate the influence of seawater pH and/or [CO_3^{2-}] on night and day Mg/Ca band compositions. The largest difference in Mg/Ca ratios occurs in the 20 °C high-Mg night bands (Fig. 4b). In that case, whole-shell Mg/Ca ratios show a significant ($p < 0.05$) decrease of 14% for day or night elevated pH groups, compared to tests grown in ambient seawater. Differences among the high Mg bands in the 25 °C groups are not significant. Low Mg day bands show a statistically significant difference ($p < 0.01$) between ambient tests and tests from the group with elevated pH during the day. Importantly, the results observed here are consistent with previous observations from bulk solution

Table 3
LA-ICP-MS data from multiple ablation depth profiles in *O. universa* from ambient seawater at 20 °C.

Sample[a]	Experiment (Amb – ambient sw) (BaN – night spike)	Min Mg/Ca (mmol mol^{-1})	Max Mg/Ca (mmol mol^{-1})	Mean Mg/Ca (mmol mol^{-1})	Mg/Ca ±2 s.e.	Mean Ba/Ca[c] (μmol mol^{-1})
103-a1-1[b]	Amb	2.7	10.7	5.6		0.55
103-a1-2[b]	Amb	2.5	11.5	6.3		0.58
103-a1-3[b]	Amb	2.8	9.5	5.9		0.58
103-b1-1[b]	Amb	2.8	10.6	5.9		0.55
103-b1-2[b]	Amb	2.9	12.3	6.1		0.56
103a1[b]	Amb	3.1	10.0	6.3		0.70
103a2[b]	Amb	2.7	11.7	5.9		0.69
103 average ±2 s.e.; n=7		***2.8±0.1***	***10.9±0.7***	***6.0±0.2***		***0.60±0.05***
342a1	Amb + 12 h BaN	3.4	9.9	6.1	0.12	
342a2	Amb + 12 h BaN	3.2	10.6	6.0	0.17	
342a3	Amb + 12 h BaN	3.7	9.8	6.1	0.14	
342b1	Amb + 12 h BaN	5.1	8.4	6.7	0.08	
342b2	Amb + 12 h BaN	5.4	8.1	6.7	0.08	
342b3	Amb + 12 h BaN	5.2	8.7	6.9	0.10	
342[d] average ±2 s.e., n=6		***4.3±0.4***	***9.3±0.4***	***6.4±0.2***	***0.12***	
344a1	Amb + 12 h BaN	3.5	10.8	6.5	0.19	
344a2	Amb + 12 h BaN	3.1	13.2	6.8	0.26	
344a3	Amb + 12 h BaN	3.1	11.0	6.4	0.19	
344b1	Amb + 12 h BaN	3.3	11.5	6.6	0.19	
344b2	Amb + 12 h BaN	3.5	11.0	6.6	0.20	
344b3	Amb + 12 h BaN	4.1	9.4	6.6	0.15	
344[d] average ±2 s.e.; n=6		***3.4±0.2***	***11.2±0.5***	***6.6±0.1***	***0.20***	

[a] a and b denote test fragments profiled; suffix denotes ablation hole (e.g. a2 = 1st fragment, 2nd hole).
[b] Data correspond to plots in Suppl. Fig. 1.
[c] Ba/Ca data are not included for Ba-spike experiments.
[d] Specimens 342 and 344 did not initiate sphere formation in the laboratory; they were collected with ~one-day-old spherical chambers.

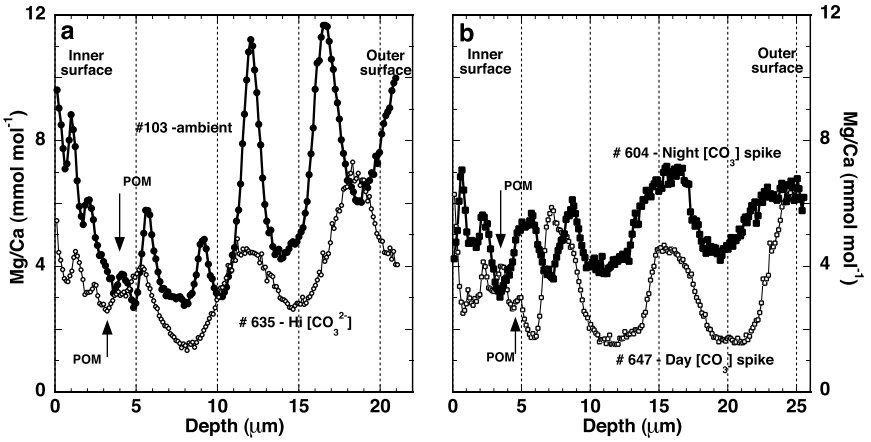

Fig. 3. Influence of elevated $[CO_3^{2-}]$ on *O. universa* test Mg/Ca grown at 20 °C on a 12 h:12 h light:dark cycle. (a) Tests grown continuously in either ambient seawater (dark closed symbols, $[CO_3^{2-}] = 177$ μmol kg^{-1}; mean Mg/Ca = 5.9 mmol mol^{-1}) or in seawater at elevated pH (open symbols, $[CO_3^{2-}] = 307$ μmol kg^{-1}; mean Mg/Ca = 3.6 mmol mol^{-1}). Note the decrease in Mg/Ca band amplitude and absolute ratios in elevated $[CO_3^{2-}]$. (b) *O. universa* grown in seawater with $[CO_3^{2-}]$ elevated to 307 μmol kg^{-1} for 12 h each night (dark closed symbols; mean Mg/Ca = 5.1 mmol mol^{-1}) or 12 h each day (open symbols; mean Mg/Ca = 3.3 mmol mol^{-1}).

ICP-MS analyses of multiple tests from laboratory experiments (Lea et al., 1999; Russell et al., 2004).

3.4. Effect of temperature on Mg/Ca band ratios

As noted earlier, the influence of temperature on foraminifer bulk test Mg/Ca composition has been documented from laboratory culture, plankton tows, and fossil material. Fig. 5 demonstrates that the Mg/Ca ratio of both low and high Mg bands in an *O. universa* test increase as calcification temperature rises. However, individual test Mg/Ca compositions vary considerably within experiments despite tight control of experimental temperatures to ±0.2 °C. For the 20 °C and 25 °C ambient seawater groups, we observe mean ratios (±1 s.d.) for the low Mg/Ca ratio bands of 2.9 ± 0.09 and 5.7 ± 1.8 mmol mol^{-1} respectively (Fig. 6a), which translates to a similar relative standard deviation (rsd) of ±31–32% for the two experiments. Variability among the high Mg/Ca ratio bands is higher in terms of absolute ratios at 10.8 ± 2.6 and 12.9 ± 3.5 mmol mol^{-1} for 20 °C and 25 °C, respectively (Fig. 6b), but in terms of rsd, the variability is reduced to 24–27%. Despite variability of low and high Mg/Ca band compositions among and between tests, when data from all specimens are combined, the average test Mg/Ca ratios are 5.9 ± 0.3 mmol mol^{-1} (±1 s.e.; $n = 21$) for the 20 °C group and 8.9 ± 0.6 ($n = 18$) for the 25 °C group (Fig. 6c). These ratios are in excellent agreement with composition estimates derived from the experimental calibration of Russell et al. (2004) based on solution ICP-MS analysis of bulk test compositions. Given a Mg/Ca-thermometer sensitivity of ~9% per °C, the 2σ standard error computed here translates to a temperature uncertainty of ±1.0 to 1.3 °C for pooled shell

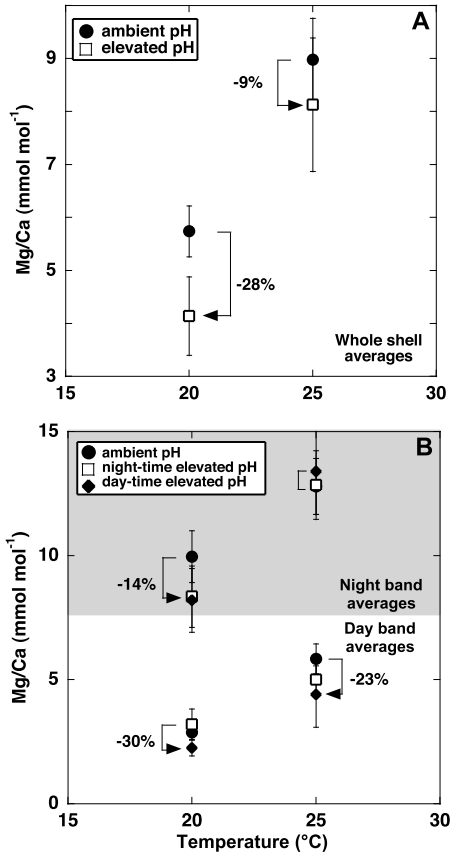

Fig. 4. Comparison of group Mg/Ca data (group mean ±2 s.e.) versus temperature and pH_{sws}. (a) Average whole shell Mg/Ca versus temperature and pH_{sws}, (b) average high (maximum ratios in each specimen) and low (minimum ratios in each specimen) band Mg/Ca versus temperature and pH_{sws}.

compositions. This is notable for being similar to estimates for the biological and environmental contribution to the uncertainty of temperature estimates obtained from the analysis of 20 individual *G. ruber* tests (Sadekov et al., 2008), although somewhat smaller than the Mg/Ca temperature uncertainty determined for the benthic foraminifera, *Ammonia tepida* (de Nooijer et al., 2014).

4. Discussion

4.1. Mg/Ca banding

A variety of explanations have been proposed to explain the existence of intrashell Mg/Ca banding in foraminifera tests (Eggins et al., 2003, 2004; Fehrenbacher and Martin, 2014; Hathorne et al., 2009; Kunioka et al., 2006; Sadekov et al., 2009, 2005). Our results demonstrate that Mg banding in *O. universa* is modulated by the light:dark cycle and is an inherent component of biomineralization in this species. Some researchers have suggested that organic layers are responsible for Mg banding in planktic foraminifers (Dueñas-Bohórquez et al., 2011; Kunioka et al., 2006). However, transmission electron microscopy (TEM) shows that in living *O. universa*, organic layers only occur on inner and outer surfaces in addition to an intratest layer that is associated with the initial biomineralization surface or primary organic membrane (POM) (Spero, 1988). Clearly, the presence of multiple high-Mg layers, corresponding to night-time growth increments in *O. universa* tests, precludes a link to internal organic layers. Moreover, LA-ICP-MS, NanoSIMS, (Figs. 1 and 2) and electron microprobe (Eggins et al., 2004) results reveal that the POM is associated with a region of low Mg/Ca composition, thereby arguing against a link between intratest organics and high Mg bands. Based on data collected here, we conclude that intratest organic layers are not the source for Mg/Ca banding in *O. universa*.

It is tempting to hypothesize that banding is controlled by the symbiont photosynthesis–respiration system through a diurnal oscillation in microenvironment pH (Jørgensen et al., 1985; Köhler-Rink and Kühl, 2005; Rink et al., 1998). However our results, based on carbonate system variations (Fig. 4a, b), cannot explain the 200–400% change in Mg that is observed in LA-ICP-MS and NanoSIMS analyses across a diurnal cycle. Interestingly, NanoSIMS imaging of the internal structure of high-Mg night bands (Fig. 1c) shows that the bands are not homogeneous. Rather, a mid-band Mg maximum is observed that is difficult to reconcile with a symbiont photosynthetic mechanism, as microenvironment pH should decrease immediately after light has been extinguished (Rink et al., 1998). For these reasons, we do not favor a photosynthesis mechanism to explain Mg banding.

Bentov and Erez (2006) reviewed potential mechanisms for Mg control in foraminifera tests and concluded that bilamellar perforate foraminifera, which include all planktic foraminifera, must actively decrease the free Mg^{2+} (relative to free Ca^{2+}) in the calcifying fluid from which the test is precipitated. Planktic foraminiferal Mg/Ca ratios are much lower than inorganic calcite precipitated in seawater (0.1–0.2 mol mol^{-1} vs. 0.002–0.01 mol mol^{-1} in foraminiferal calcite) (Oomori et al., 1987), thereby suggesting the activity ratio of Mg^{2+} to Ca^{2+} in the calcifying fluid is reduced by ~90 to 99% relative to ambient seawater. This could be achieved by either importing Ca^{2+} ions or exporting even more Mg^{2+} ions from the calcifying fluid in order to regulate free [Mg^{2+}] and [Ca^{2+}] activities to the levels inferred from the low Mg/Ca composition of a foraminifera test.

Bentov and Erez (2006) postulated an arrangement of plausible ion channels and pumps to regulate ion concentrations within the calcifying fluid, that are organized so that Mg^{2+} activity is reduced and pH increased. Their model invokes a directed flux of Mg^{2+} through the cell, with Mg^{2+} being removed from the calcifying fluid into the cell and subsequently expelled to external seawater. Mg^{2+} removal from the calcifying fluid is attributed to either Mg^{2+}–Ca^{2+} antiports and/or Mg^{2+}-specific channels. In the latter case, Mg^{2+} uptake by the cell is driven by electrochemical gradients that are generated via a Na^{+}–H^{+} antiporter, which simultaneously raises pH within the calcifying fluid. Mg^{2+} efflux from the foraminifer cell is attributed to one or more plausible antiporters ($2Na^{+}$–Mg^{2+}, $2H^{+}$–Mg^{2+}, or Ca^{2+}–Mg^{2+}) or a Mg^{2+}-pump linked to ATP hydrolysis (see Fig. 2, Bentov and Erez, 2006) that is located in the cell's external membrane. In addition, Bentov and Erez (2006) point out a possible role for internal organelles, specifically the mitochondria and endoplasmic reticulum, in controlling Mg^{2+} removal from the calcifying fluid, based on the known capacity for mitochondria to temporarily sequester Mg^{2+}.

There is reasonable circumstantial evidence for mitochondria to play a key role in controlling Mg/Ca activity ratios in the calcification fluid. Firstly, TEM studies of planktic foraminiferal biomineralization reveal that the rhizopodia adjacent to test surfaces are dense with mitochondria, which may be oriented along the periphery of the cytoplasm volume (see Plate 6 in Bé et al., 1979; Fig. 4 in Spero, 1988). Mitochondria are critical to the regulation of cellular Mg^{2+} levels and have a very high capacity Mg^{2+} uptake system. They contain Mg^{2+}-specific Mrs2p protein channels that are located in the inner mitochondrial membrane (Schindl et al., 2007). These channels select for Mg^{2+} based on the large diameter of the fully hydrated Mg^{2+} ion (4.7 Å), and can facilitate rapid Mg^{2+} uptake across the inner mitochondrial membrane due to a counter flux of H^{+} ions, which sustains a very negative transmembrane potential ($\Delta\Psi$) of −155 mV. In theory, this potential could support a Mg^{2+} concentration in excess of 1 M within the

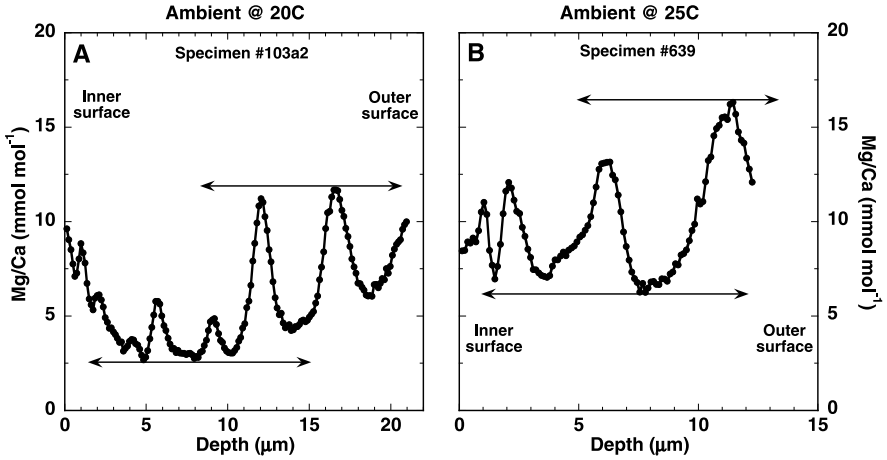

Fig. 5. Comparison of LA-ICP-MS profile through an *O. universa* maintained at (a) 20 °C and (b) 25 °C. Note that both the high and low Mg/Ca band ratios increase with temperature.

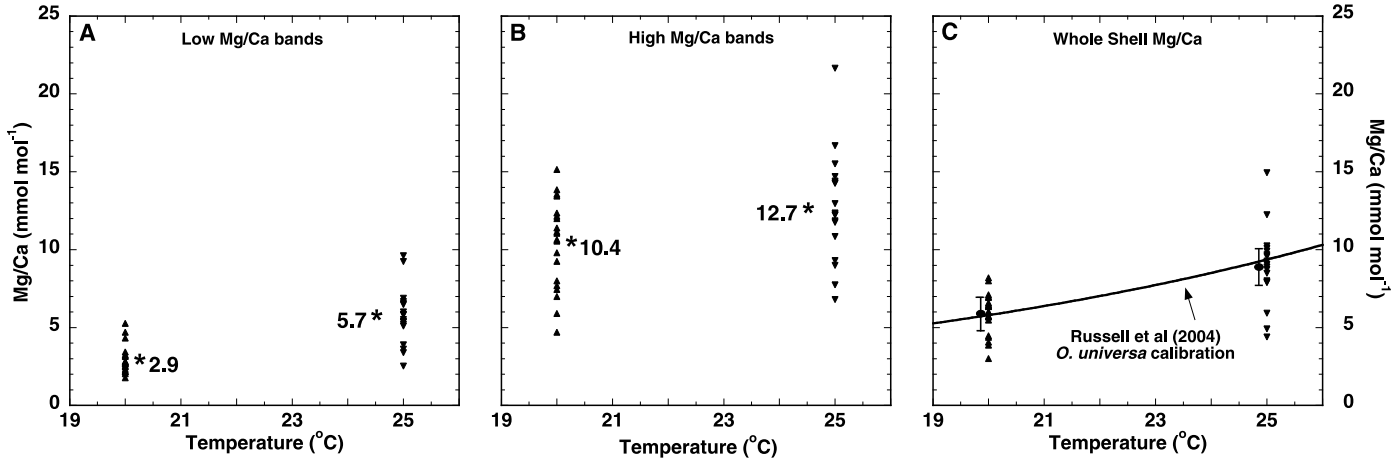

Fig. 6. Summary plot of Mg/Ca averages of ablation holes from individual *O. universa* in Suppl. Table 1. All foraminifera were grown in ambient seawater without carbonate chemistry modification at 20 °C ($n = 21$) or 25 °C ($n = 18$). Plotted data for the 20 °C and 25 °C groups include specimens from groups Amb-20, BD20, BN20, BC20 and BD25, BN25, BC25. (a) Low Mg/Ca band minimum ratios, (b) high Mg/Ca band maximum ratios, (c) average Mg/Ca ratios for whole shells. The averages of low and high Mg bands are indicated in (a) and (b) by black asterisks and average values; population averages in (c) are shown to the left of the shell data. Note that population averages are within 5–6% (±1 s.e.; = ±0.5 °C) of the predicted Mg/Ca ratios for this species (regression line) based on bulk solution analyses of multiple foraminifer shells grown in culture (Russell et al., 2004).

inner mitochondrial space, although most dissolved Mg is complexed and only a small fraction occurs as free Mg^{2+} (0.4–0.8 nM; Schindl et al., 2007).

We hypothesize that either light-triggered variation in Mg^{2+}-uptake by mitochondria, or possibly diurnal changes in mitochondrial abundance or activity in the vicinity of the calcifying surfaces or both, may account for the diurnal Mg/Ca banding cycles observed in *O. universa* and perhaps other planktic foraminifera. Our hypothesis differs from that previously proposed for Mg^{2+}-banding in the benthic foraminifer *Amphistegina lobifera* (Bentov and Erez, 2005). These authors proposed that Mg/Ca banding in *A. lobifera* and other foraminifera may be due to alternating calcification of a phosphorous-rich, high-Mg^{2+} calcium carbonate phase, referred to as primary calcite, and a low Mg^{2+} secondary calcite phase. Bentov and Erez (2005) observed the high Mg^{2+} phase in *A. lobifera* to be associated with initial chamber wall formation and the POM, but this conflicts with previous observations (Sadekov et al., 2005) and results here which show that the *O. universa* POM is a site of low Mg composition (Figs. 1c and 2a). These conflicting observations suggest there may be fundamental differences in biomineralization mechanisms between some benthic and planktic species.

If seawater diffusion into the calcifying fluid between rhizopodia and the test surface replenishes some Mg^{2+}, perhaps a temperature-dependent increase in diffusion rates from the adjacent seawater environment to the site of calcification contributes to the observed temperature sensitivity of the Mg/Ca thermometer. Such a mechanism, while speculative, would also be compatible with the seawater vacuolization model that has been proposed to explain cation transport to calcification sites in benthic foraminifera (Bentov et al., 2009). Alternatively, Mg/Ca temperature sensitivity could be influenced by a Q10 type effect on mitochondrial membrane Mg^{2+} transport.

4.2. Interspecies differences in Mg/Ca ratios

Several previous studies have examined Mg heterogeneity in foraminifera tests in an attempt to improve our understanding of the Mg/Ca thermometer (de Nooijer et al., 2014; Dueñas-Bohórquez et al., 2011; Sadekov et al., 2005, 2008, 2009). Our results show that considerable Mg/Ca variation exists within and between individual tests that are grown under constant temperature conditions in culture. In *O. universa*, differences between individuals appear to be magnified in the high-Mg night bands relative to the low-Mg day bands. LA-ICP-MS and NanoSIMS also show elevated Mg/Ca in both high and low Mg bands near the outer test surfaces (Figs. 1c and 2), which is not due to organics

in the test wall. This effect is most obvious in the outermost bands of long-lived *O. universa* that thicken their tests for many (6–8) days (e.g. Fig. 1c), indicating these specimens may develop higher Mg/Ca compositions at a given temperature than shorter lived individuals. Estimates for *O. universa* sphere thickening in culture ranges from ~2–9 days in the northeast Pacific in the vicinity of Catalina Island (Spero, 1988), to ~5–6 days in the Caribbean near Barbados and Curaçao (Caron et al., 1987). Such tests correspond to the thin-walled variety (Billups and Spero, 1995; Deuser et al., 1981) with thicknesses between 10–30 μm, and likely exhibit Mg heterogeneity characteristic of specimens used for past Mg/Ca laboratory calibrations (Lea et al., 1999; Russell et al., 2004).

The high Mg/Ca compositions of *O. universa* tests compared with other species have been noted previously from core-top and sediment-trap assemblages (Anand et al., 2003). As such, *O. universa* is often regarded as an anomaly among planktic species although the sensitivity of the Mg/Ca-temperature relationship in *Orbulina* is similar to other planktic species. Whereas the pattern of ontogenetic test development versus spherical chamber thickening is a significant distinction between *O. universa* and other species, there are important similarities that allow us to extend our observations beyond *Orbulina*. Our Ba^{2+} labeling experiments demonstrate that the high Mg bands in *O. universa* are produced at night. Average *Orbulina* Mg/Ca ratios may be elevated because the sphere calcifies for ~2–9 days, and 30% of the test calcite is precipitated at night (Lea et al., 1995; Spero and Parker, 1985).

Electron microprobe images of multi-chambered species such as *G. ruber, G. sacculifer, G. conglobatus, N. dutertrei, G. inflata, G. scitula* and *G. menardii* (Hathorne et al., 2009; Sadekov et al., 2005) show that chambers are composed primarily of low Mg calcite with relatively thin bands of high Mg calcite tending to be located nearer the inner surfaces of the test. An interesting aspect of foraminifer chamber calcification that has only been rarely reported (Hemleben et al., 1985; Spero, 1988) is that initial chamber formation in *O. universa, G. ruber, G. sacculifer, G. bulloides, G. menardii* and other species generally begins late at night. New specimens brought into the lab after early scuba collection dives (before 08:00 h) often have glassy, thinly-calcified chambers on the tests (Spero, unpub. observation). During the subsequent 12 h, these chambers take on an opaque appearance that indicates progressive calcification and thickening, after which cytoplasm expands into the new chamber. These observations suggest that most chamber thickening occurs during the day, and by analogy with *O. universa*, should be composed primarily of low Mg calcite with thin high Mg layers near the inner chamber wall. Assuming this interpretation of Mg banding in multichambered species, microprobe (Sadekov et al., 2005) and LA-ICP-MS evidence (Sadekov et al., 2008, 2010) would be consistent with chamber formation and thickening comprising 80–90% of low Mg, daytime type, and 10–20% of thin, high-Mg night-time type.

4.3. Implications for paleoceanographic applications

Mg/Ca paleothermometry has been utilized for nearly 15 years to reconstruct past ocean temperatures from fossil foraminifera, yet our knowledge of how the thermometer works is empirical and has been challenged by the presence of unexplained intra- and intertest Mg/Ca variations. Here, we demonstrate that the Mg/Ca ratios of both the high and low Mg bands in *O. universa* increase with increasing temperature (Figs. 5a and 5b) and that the average Mg/Ca compositions of tests grown at 20 °C and 25 °C agree with previous bulk solution laboratory calibrations for this species (Russell et al., 2004) (Fig. 6c). These results indicate consistency between LA-ICP-MS microanalysis estimates and solution-based ICP-MS bulk test compositions, and demonstrate that intratest compositional heterogeneity is an inherent and reproducible feature of foraminiferal calcification that does not compromise the application of the Mg/Ca paleothermometer for paleoceanographic reconstructions.

Laboratory (Kisakürek et al., 2008; Lea et al., 1999; Nürnberg et al., 1996; Russell et al., 2004), sediment trap (Anand et al., 2003; McConnell and Thunell, 2005) and core top (Dekens et al., 2002; Groeneveld and Chiessi, 2011) studies have produced multi-species and species-specific calibrations for interpreting Mg/Ca data. A common feature in all these studies is that calibration material was derived from foraminifer tests that had completed their lifecycle and undergone gametogenesis. Hence, each test contained a full life cycle of Mg/Ca banding. These calibration studies also benefit from the bulk solution-based analysis of a number of tests ($n = 5$–50), thereby producing robust calibrations that integrate intratest and intertest differences in a population. Many studies during the past decade have confirmed the robustness and wide applicability of these solution-based Mg/Ca calibrations.

With the expanding use of microanalytical techniques to quantify metal/Ca ratios in different chambers of individual foraminifers, some studies have begun to develop and apply Mg/Ca versus temperature calibrations for particular chambers within a species (Dueñas-Bohórquez et al., 2011; Marr et al., 2011). Similarly, researchers are exploring the application of plankton-tow derived material for Mg:T calibrations (van Raden et al., 2011). However, plankton tow calibrations have a significant drawback. Most important, unless empty at collection, the tests being analyzed have not completed their life cycle and therefore do not contain the full complement of chambers and Mg banding in their tests. The lack of a final calcification phase in calibration material would likely result in tests having different Mg/Ca ratios than fossil material that reflects individuals with complete life cycles. Similarly, chamber-based calibrations may be useful for capturing environmental conditions during a particular life-stage of a species. However, the depth habitat and/or seasonal significance of the geochemistry of a single chamber is difficult to constrain without careful analyses of material from sediment traps in conjunction with water column MOCNESS tows that constrain species depth preferences (Curry et al., 1983; Fairbanks et al., 1982). Given these uncertainties, Mg/Ca calibrations using plankton tow material or chamber-specific calibrations should be applied with caution.

From a paleoceanographic perspective, the information one can collect on the Mg/Ca ratios of a population of individual foraminifera shells is intriguing because it could provide information on seasonal and depth habitat temperature extremes (Haarmann et al., 2011; Laepple and Huybers, 2013; Wit et al., 2010), analogous to earlier studies using oxygen and carbon isotopes (Billups and Spero, 1995, 1996; Koutavas et al., 2006; Spero and Williams, 1989). With the broad array of geochemical proxy calibrations available for *O. universa* (Bemis et al., 1998; Hönisch et al., 2011; Lea et al., 1999; Mashiotta et al., 1997; Russell et al., 2004; Sanyal et al., 1996) and its large range of temperature and salinity tolerances (Bijma et al., 1990), this species may be unique in its ability to record temperature, salinity and other physical parameters of the mixed layer and upper thermocline between 40°N–40°S latitudes (Bé, 1977).

A clear conclusion that can be drawn from this study is that LA-ICP-MS analyses on individual foraminifera have the potential to yield novel information from the paleoceanographic record, but that these data should be interpreted within the context of a population of tests. Applications that utilize Mg/Ca data from individual tests need to evaluate population outliers carefully because they may not yield environmentally relevant information. Nevertheless, LA-ICP-MS is a valuable technique for exploring calcification mechanisms in foraminifers and other calcifying organisms as well as

exploring new applications for individual test geochemistry for paleoceanographic applications.

5. Conclusions

In this study, we have presented results from a laser ablation study of the planktic foraminifer *O. universa* that was grown in laboratory experiments to elucidate the timing and mechanism of intrashell Mg/Ca banding during test calcification. We demonstrate that high Mg bands are precipitated at night whereas low Mg bands are precipitated during the day. Changes in carbonate chemistry, and by analogy in symbiont photosynthesis, have an affect on the amplitude and thickness of the Mg bands does not appear to explain or account for the Mg magnitude and heterogeneity observed in the high Mg bands. We suggest a mechanism to explain the development of Mg-banding that is tied to the light:dark cycle and involves mitochondrial uptake of Mg from a calcification space beneath rhizopodia on the test surface. Experimental data show that both high and low Mg bands exhibit increased Mg/Ca with increasing temperature, and that the average Mg/Ca ratios of individual *O. universa* tests derived from LA-ICP-MS measurements agree well with previous empirical calibration studies using solution-based ICP-MS analyses on multiple foraminifera tests.

Acknowledgements

We gratefully acknowledge the comments of two anonymous reviewers, and the assistance of S. Alford, S. Doo, R. da Rocha, A. Kuroyanagi, D. Winter, G. Nash, and the staff of the Wrigley Marine Science Center for field, laboratory and analytical assistance with the experiments and analyses described in this study, and to A. Sadekov and K. Kimoto for their contributions to the culture and NanoSIMS imaging of the foraminifer illustrated in Fig. 1c. The authors also acknowledge the facilities and scientific and technical assistance of the Australian Microscopy & Microanalysis Research Facility at the Centre for Microscopy, Characterisation & Analysis and The University of Western Australia, a facility funded by the University, State and Commonwealth Governments. This research was supported with awards from the U.S. National Science Foundation, OCE-0550703 (HJS) and OCE-0751764 (BH), and the Australian Research Council, DP0880010 (SME).

Appendix A. Supplementary material

Supplementary material related to this article can be found online at http://dx.doi.org/10.1016/j.epsl.2014.10.030.

References

Anand, P., Elderfield, H., 2005. Variability of Mg/Ca and Sr/Ca between and within the planktonic foraminifers *Globigerina bulloides* and *Globorotalia truncatulinoides*. Geochem. Geophys. Geosyst. 6, Q11D15. http://dx.doi.org/10.1029/2004gc000811.

Anand, P., Elderfield, H., Conte, M.H., 2003. Calibration of Mg/Ca thermometry in planktonic foraminifera from a sediment trap time series. Paleoceanography 18 (2), 1050. http://dx.doi.org/10.1029/2002PA000846.

Arbuszewski, J., deMenocal, P., Kaplan, A., Farmer, E.C., 2010. On the fidelity of shell-derived $\delta^{18}O_{seawater}$ estimates. Earth Planet. Sci. Lett. 300, 185–196.

Australian Microscopy and Microanalysis Research Facility, 2008. AMMRF 2008 Profile Report. AMMRF, Sydney. 30 pp.

Bé, A.W.H., 1977. An ecological, zoogeographic and taxonomic review of recent planktonic foraminifera. In: Ramsay, A.T.S. (Ed.), Oceanic Micropaleontology. Academic Press, London, pp. 1–100.

Bé, A.W.H., Hemleben, C., Anderson, O.R., Spindler, M., 1979. Chamber formation in planktonic foraminifera. Micropaleontology 25, 294–307.

Bé, A.W.H., Anderson, O.R., Faber Jr., W.W., Caron, D.A., 1983. Sequence of morphological and cytoplasmic changes during gametogenesis in the planktonic foraminifer *Globigerinoides sacculifer* (Brady). Micropaleontology 29, 310–325.

Bemis, B.E., Spero, H.J., Bijma, J., Lea, D.W., 1998. Reevaluation of the oxygen isotopic composition of planktonic foraminifera: experimental results and revised paleotemperature equations. Paleoceanography 13, 150–160.

Bentov, S., Erez, J., 2005. Novel observations on biomineralization processes in foraminifera and implications for Mg/Ca ratio in the shells. Geology 33, 841–844.

Bentov, S., Erez, J., 2006. Impact of biomineralization processes on the Mg content of foraminiferal shells: a biological perspective. Geochem. Geophys. Geosyst. 7. http://dx.doi.org/10.1029/2005GC001015.

Bentov, S., Bronwnlee, C., Erez, J., 2009. The role of seawater endocytosis in the biomineralization process in calcareous foraminifera. Proc. Natl. Acad. Sci. USA 106, 21500–21504.

Bijma, J., Faber Jr., W.W., Hemleben, C., 1990. Temperature and salinity limits for growth and survival of some planktonic foraminifers in laboratory cultures. J. Foraminiferal Res. 20, 95–116.

Billups, K., Spero, H.J., 1995. Relationship between shell size, thickness and stable isotopes in individual planktonic foraminifera from two equatorial Atlantic cores. J. Foraminiferal Res. 25, 24–37.

Billups, K., Spero, H.J., 1996. Reconstructing the stable isotope geochemistry and paleotemperatures of the equatorial Atlantic during the last 150,000 years: results from individual foraminifera. Paleoceanography 11, 217–238.

Brown, S.J., Elderfield, H., 1996. Variations in Mg/Ca and Sr/Ca ratios of planktonic foraminifera caused by postdepositional dissolution: evidence of shallow Mg-dependent dissolution. Paleoceanography 11, 543–551.

Caron, D.A., Faber Jr., W.W., Bé, A.W.H., 1987. Growth of the spinose planktonic foraminifer *Orbulina universa* in laboratory culture and the effect of temperature on life processes. J. Mar. Biol. Assoc. UK 67, 343–358.

Church, T.M., Wolgemuth, K., 1972. Marine barite saturation. Earth Planet. Sci. Lett. 15, 35–44.

Curry, W.B., Thunell, R.C., Honjo, S., 1983. Seasonal changes in the isotopic composition of planktonic foraminifera collected in Panama Basin sediment traps. Earth Planet. Sci. Lett. 64, 33–43.

Davis, K.J., Dove, P.M., Wasylenki, L.E., de Yoreo, J.J., 2004. Morphological consequences of differential Mg^{2+} incorporation at structurally distinct steps on calcite. Am. Mineral. 89, 714–720.

Dekens, P.S., Lea, D.W., Pak, D.K., Spero, H.J., 2002. Core top calibration of Mg/Ca in tropical foraminifera: refining paleo-temperature estimation. Geochem. Geophys. Geosyst. 3. http://dx.doi.org/10.1029/2001GC000200.

de Nooijer, L.J., Hathorne, E.C., Reichart, G.J., Langer, G., Bijma, J., 2014. Variability in calcitic Mg/Ca and Sr/Ca ratios in clones of the benthic foraminifer *Ammonia tepida*. Mar. Micropaleontol. 107, 32–43.

Deuser, W.G., Ross, E.H., Hemleben, C., Spindler, M., 1981. Seasonal changes in species composition, numbers, mass, size, and isotopic composition of planktonic foraminifera settling into the deep Sargasso Sea. Palaeogeogr. Palaeoclimatol. Palaeoecol. 33, 103–127.

Dickson, Andrew G., 1990. Standard potential of the reaction: $AgCl(s) + 1/2H_2(g) = Ag(s) + HCl(aq)$, and the standard acidity constant of the ion HSO_4^- in synthetic sea water from 273.15 to 318.15 K. J. Chem. Thermodyn. 22 (2), 113–127.

Dickson, A.G., Millero, F.J., 1987. A comparison of the equilibrium constants for the dissociation of carbonic acid in seawater media. Deep-Sea Res. 34, 1733–1743.

Dueñas-Bohórquez, A., da Rocha, R.E., Kuroyanagi, A., de Nooijer, L.J., Bijma, J., Reichart, G.J., 2011. Interindividual variability and ontogenetic effects on Mg and Sr incorporation in the planktonic foraminifer *Globigerinoides sacculifer*. Geochim. Cosmochim. Acta 75, 520–532.

Eggins, S.M., Kinsley, L.K., Shelley, J.M.G., 1998. Deposition and element fractionation processes during atmospheric sampling for analysis by ICPMS. Appl. Surf. Sci. 127–129, 278–286.

Eggins, S., Deckker, P.D., Marshall, J., 2003. Mg/Ca variation in planktonic foraminifera tests: implications for reconstructing palaeo-seawater temperature and habitat migration. Earth Planet. Sci. Lett. 212, 291–306.

Eggins, S.M., Sadekov, A., De Deckker, P., 2004. Modulation and daily banding of Mg/Ca in *Orbulina universa* tests by symbiont photosynthesis and respiration: a complication for seawater thermometry? Earth Planet. Sci. Lett. 225, 411–419.

Elderfield, H., Ganssen, G., 2000. Past temperature and $\delta^{18}O$ of surface ocean waters inferred from foraminiferal Mg/Ca ratios. Nature 405, 442–445.

Elderfield, H., Bertram, C.J., Erez, J., 1996. A biomineralization model for the incorporation of trace elements into foraminiferal calcium carbonate. Earth Planet. Sci. Lett. 142, 409–423.

Erez, J., 2003. The source of ions for biomineralization in foraminifera and their implications for paleoceanographic proxies. In: Dove, P.M., De Yoreo, J.J., Weiner, S. (Eds.), Biomineralization. Mineralogical Society of America/Geochemical Society, pp. 115–149.

Fairbanks, R.G., Sverdlove, M., Free, R., Wiebe, P.H., Bé, A.W.H., 1982. Vertical distribution and isotopic fractionation of living planktonic foraminifera from the Panama Basin. Nature 298, 841–844.

Fehrenbacher, J., Martin, P., 2010. Mg/Ca variability of the planktonic foraminifera *G. ruber s.s.* and *N. dutertrei* from shallow and deep cores determined by electron microprobe image mapping. In: PAGES 1st Young Scientists Meeting (YSM) – 'Retrospective Views on our Planet's Future', vol. 9. 012018.

Fehrenbacher, J., Martin, P., 2014. Exploring the dissolution effect on the intrashell Mg/Ca variability of the planktic foraminifer *Globigerinoides ruber*. Paleoceanography 29, 854–868. http://dx.doi.org/10.1002/2013PA002571.

Gastrich, M.D., 1987. Ultrastructure of a new intracellular symbiotic alga found within planktonic foraminifera. J. Phycol. 23, 623–632.

Groeneveld, J., Chiessi, C.M., 2011. Mg/Ca of *Globorotalia inflata* as a recorder of permanent thermocline temperatures in the South Atlantic. Paleoceanography 26, PA2203.

Haarmann, T., Hathorne, E.C., Mohtadi, M., Groeneveld, J., Kolling, M., Bickert, T., 2011. Mg/Ca ratios of single planktonic foraminifer shells and the potential to reconstruct the thermal seasonality of the water column. Paleoceanography 26, PA3218.

Hathorne, E.C., Alard, O., James, R.H., Rogers, N.W., 2003. Determination of intratest variability of trace elements in foraminifera by laser ablation inductively coupled plasma-mass spectrometry. Geochem. Geophys. Geosyst. 4.

Hathorne, E.C., James, R.H., Lampitt, R.S., 2009. Environmental versus biomineralization controls on the intratest variation in the trace element composition of the planktonic foraminifera *G. inflata* and *G. scitula*. Paleoceanography 24, PA4204.

Hemleben, C., Spindler, M., Breitinger, I., Deuser, W.G., 1985. Field and laboratory studies on the ontogeny and ecology of some Globorotaliid species from the Sargasso Sea off Bermuda. J. Foraminiferal Res. 15, 254–272.

Hönisch, B., Allen, K.A., Russell, A.D., Eggins, S.M., Bijma, J., Spero, H.J., Lea, D.W., Yu, J., 2011. Planktic foraminifers as recorders of seawater Ba/Ca. Mar. Micropaleontol. 79, 52–57.

Hönisch, B., Allen, K.A., Lea, D.W., Spero, H.J., Eggins, S.M., Arbuszewski, J., deMenocal, P., Rosenthal, Y., Russell, A.D., Elderfield, H., 2013. The influence of salinity on Mg/Ca in planktic foraminifers – evidence from cultures, core-top sediments and complementary $\delta^{18}O$. Geochim. Cosmochim. Acta 121, 196–213.

Jørgensen, B.B., Erez, J., Revsbech, N.P., Cohen, Y., 1985. Symbiotic photosynthesis in a planktonic foraminiferan, *Globigerinoides sacculifer* (Brady), studied with microelectrodes. Limnol. Oceanogr. 30, 1253–1267.

Kisakürek, B., Eisenhauer, A., Böhm, F., Garbe-Schönberg, D., Erez, J., 2008. Controls on shell Mg/Ca and Sr/Ca in cultured planktonic foraminiferan, *Globigerinoides ruber* (white). Earth Planet. Sci. Lett. 273, 260–269.

Köhler-Rink, S., Kühl, M., 2005. The chemical microenvironment of the symbiotic planktonic foraminifera *Orbulina universa*. Marine Biol. Res. 1, 68–78.

Koutavas, A., deMenocal, P.B., Olive, G.C., Lynch-Steiglitz, J., 2006. Mid-Holocene El Nino-Southern Oscillation (ENSO) attenuation revealed by individual foraminifera in eastern tropical Pacific sediments. Geology 34, 993–996.

Kunioka, D., Shirai, K., Takahata, N., Sano, Y., Toyofuku, T., Ujiie, Y., 2006. Microdistribution of Mg/Ca, Sr/Ca, and Ba/Ca ratios in *Pulleniatina obliquiloculata* test by using a NanoSIMS: implication for the vital effect mechanism. Geochem. Geophys. Geosyst. 7, 11.

Laepple, T., Huybers, P., 2013. Reconciling discrepancies between Uk37 and Mg/Ca reconstructions of Holocene marine temperature variability. Earth Planet. Sci. Lett. 375, 418–429.

Lea, D.W., Spero, H.J., 1992. Experimental determination of barium uptake in shells of the planktonic foraminifera *Orbulina universa* at 22 °C. Geochim. Cosmochim. Acta 56, 2673–2680.

Lea, D.W., Spero, H.J., 1994. Assessing the reliability of paleochemical tracers: barium uptake in the shells of planktonic foraminifera. Paleoceanography 9, 445–452.

Lea, D.W., Martin, P.A., Chan, D.A., Spero, H.J., 1995. Calcium uptake and calcification rate in the planktonic foraminifer *Orbulina universa*. J. Foraminiferal Res. 25, 14–23.

Lea, D.W., Mashotta, T.A., Spero, H.J., 1999. Controls on magnesium and strontium uptake in planktonic foraminifera determined by live culturing. Geochim. Cosmochim. Acta 63, 2369–2379.

Longerich, H.P., Jackson, S.E., Gunther, D., 1996. Laser ablation inductively coupled plasma mass spectrometric transient signal data acquisition and analyte concentration calculation. J. Anal. At. Spectrom. 11, 899–904.

Marr, J.P., Baker, J.A., Carter, L., Allan, A.S.R., Dunbar, G.B., Bostock, H.C., 2011. Ecological and temperature controls on Mg/Ca ratios of *Globigerina bulloides* from the southwest Pacific Ocean. Paleoceanography 26, PA2209.

Mashiotta, T.A., Lea, D.W., Spero, H.J., 1997. Experimental determination of cadmium uptake in shells of the planktonic foraminifera *Orbulina universa* and *Globigerina bulloides*: implications for surface water paleoreconstructions. Geochim. Cosmochim. Acta 61, 4053–4065.

Mathien-Blard, E., Bassinot, F., 2009. Salinity bias on the foraminifera Mg/Ca thermometry: correction procedure and implications for past ocean hydrographic reconstructions. Geochem. Geophys. Geosyst. 10, Q12011.

McConnell, M.C., Thunell, R.C., 2005. Calibration of the planktonic foraminiferal Mg/Ca paleothermometer: sediment trap results from the Guaymas Basin, Gulf of California. Paleoceanography 20, PA2016.

McKenna, V.S., Prell, W.L., 2004. Calibration of the Mg/Ca *Globorotalia truncatulinoides* (R) for the reconstruction of marine temperature gradients. Paleoceanography 19, PA2006.

Mehrbach, C., Culberson, C.H., Hawley, J.E., Pytkowicz, R.M., 1973. Measurement of the apparent dissociation constants of carbonic acid in seawater at atmospheric pressure. Limnol. Oceanogr. 18, 897–907.

Nürnberg, D., Bijma, J., Hemleben, C., 1996. Assessing the reliability of magnesium in foraminiferal calcite as a proxy for water mass temperatures. Geochim. Cosmochim. Acta 60, 803–814.

Oomori, T., Kaneshima, G., Maezato, Y., 1987. Distribution coefficient of Mg^{2+} ions between calcite and solution at 10–50 °C. Mar. Chem. 20, 327–336.

Pak, D.K., Lea, D.W., Kennett, J.P., 2004. Seasonal and interannual variation in Santa Barbara Basin water temperatures observed in sediment trap foraminiferal Mg/Ca. Geochem. Geophys. Geosyst. 5, Q12008.

Pearce, N.J.G., Perkins, W.T., Westgate, J.A., Gorton, M.P., Jackson, S.E., Neal, C.R., Chenery, S.P., 1997. A compilation of new and published major and trace element data for NIST SRM 610 and NIST SRM 612 glass reference materials. Geostand. Newsl. 21, 115–144.

Reed, W.P., 1992. Certificates of Analysis for SRMs 610–611; 612–613; 614–615; 616–617 (revised). Natl. Inst. of Stand. and Technology, Gaithersburg, USA.

Rink, S., Kühl, M., Bijma, J., Spero, H.J., 1998. Microsensor studies of photosynthesis and respiration in the symbiotic foraminifer *Orbulina universa*. Mar. Biol. 131, 583–595.

Robbins, L.L., Hansen, M.E., Kleypas, J.A., Meylan, S.C., 2010. CO2calc: a user-friendly seawater carbon calculator for Windows, Mac OSX, and IOS (iPhone). Open-File Report 2010-1280, U.S. Department of Interior. U.S. Geological Survey. 17 pages.

Rosenthal, Y., Lohmann, G.P., 2002. Accurate estimation of sea surface temperatures using dissolution-corrected calibrations for Mg/Ca paleothermometry. Paleoceanography 17, 1044.

Russell, A.D., Hönisch, B., Spero, H.J., Lea, D.W., 2004. Effects of seawater carbonate ion concentration and temperature on shell U, Mg, and Sr in cultured planktonic foraminifera. Geochim. Cosmochim. Acta 68, 4347–4361.

Sadekov, A.Y., Eggins, S.M., De Deckker, P., 2005. Characterization of Mg/Ca distributions in planktonic foraminifera species by electron microprobe mapping. Geochem. Geophys. Geosyst. 6, Q12P06.

Sadekov, A., Eggins, S.M., De Deckker, P., Kroon, D., 2008. Uncertainties in seawater thermometry deriving from intratest and intertest Mg/Ca variability in *Globigerinoides ruber*. Paleoceanography 23.

Sadekov, A., Eggins, S.M., De Deckker, P., Ninnemann, U., Kuhnt, W., Bassinot, F., 2009. Surface and subsurface seawater temperature reconstruction using Mg/Ca microanalysis of planktonic foraminifera *Globigerinoides ruber*, *Globigerinoides sacculifer*, and *Pulleniatina obliquiloculata*. Paleoceanography 24.

Sadekov, A.Y., Eggins, S.M., Klinkhammer, G.P., Rosenthal, Y., 2010. Effects of seafloor and laboratory dissolution on the Mg/Ca composition of *Globigerinoides sacculifer* and *Orbulina universa* tests – a laser ablation ICPMS microanalysis perspective. Earth Planet. Sci. Lett. 292, 312–324.

Sanyal, A., Hemming, N.G., Broecker, W.S., Lea, D.W., Spero, H.J., Hanson, G.N., 1996. Oceanic pH control on the boron isotopic composition of foraminifera: evidence from culture experiments. Paleoceanography 11, 513–517.

Schindl, R., Weghuber, J., Romanin, C., Schweyen, R.J., 2007. Mrs2p forms a high conductance Mg^{2+} selective channel in mitochondria. Biophys. J. 93, 3872–3883.

Spero, H.J., 1988. Ultrastructural examination of chamber morphogenesis and biomineralization in the planktonic foraminifer *Orbulina universa*. Mar. Biol. 99, 9–20.

Spero, H.J., Parker, S.L., 1985. Photosynthesis in the symbiotic planktonic foraminifer *Orbulina universa*, and its potential contribution to oceanic primary productivity. J. Foraminiferal Res. 15, 273–281.

Spero, H.J., Williams, D.F., 1989. Opening the carbon isotope "vital effect" black box. 1. Seasonal temperatures in the euphotic zone. Paleoceanography 4, 593–601.

Toyofuku, T., Kitazato, H., 2005. Micromapping of Mg/Ca values in cultured specimens of the high-magnesium benthic foraminifera. Geochem. Geophys. Geosyst. 6, Q11P05.

van Raden, U.J., Groeneveld, J., Raitzch, M., Kucera, M., 2011. Mg/Ca in the planktonic foraminifera *Globorotalia inflata* and *Globigerinoides bulloides* from Western Mediterranean plankton tow and core top samples. Mar. Micropaleontol. 78, 101–112.

Vetter, L., Kozdon, R., Mora, C.I., Eggins, S.M., Valley, J.W., Hönisch, B., Spero, H.J., 2013. Micron-scale intrashell oxygen isotope variation in cultured planktic foraminifers. Geochim. Cosmochim. Acta 107, 267–278.

Wit, J.C., Reichart, G.J., Jung, S.J.A., Kroon, D., 2010. Approaches to unravel seasonality in sea surface temperatures using paired single-specimen foraminiferal $\delta^{18}O$ and Mg/Ca analyses. Paleoceanography 25, PA4220.

Yu, J., Elderfield, H., 2008. Mg/Ca in the benthic foraminifera *Cibicidoides wuellerstorfi* and *Cibicidoides mundulus*: temperature versus carbonate ion saturation. Earth Planet. Sci. Lett. 276, 129–139.

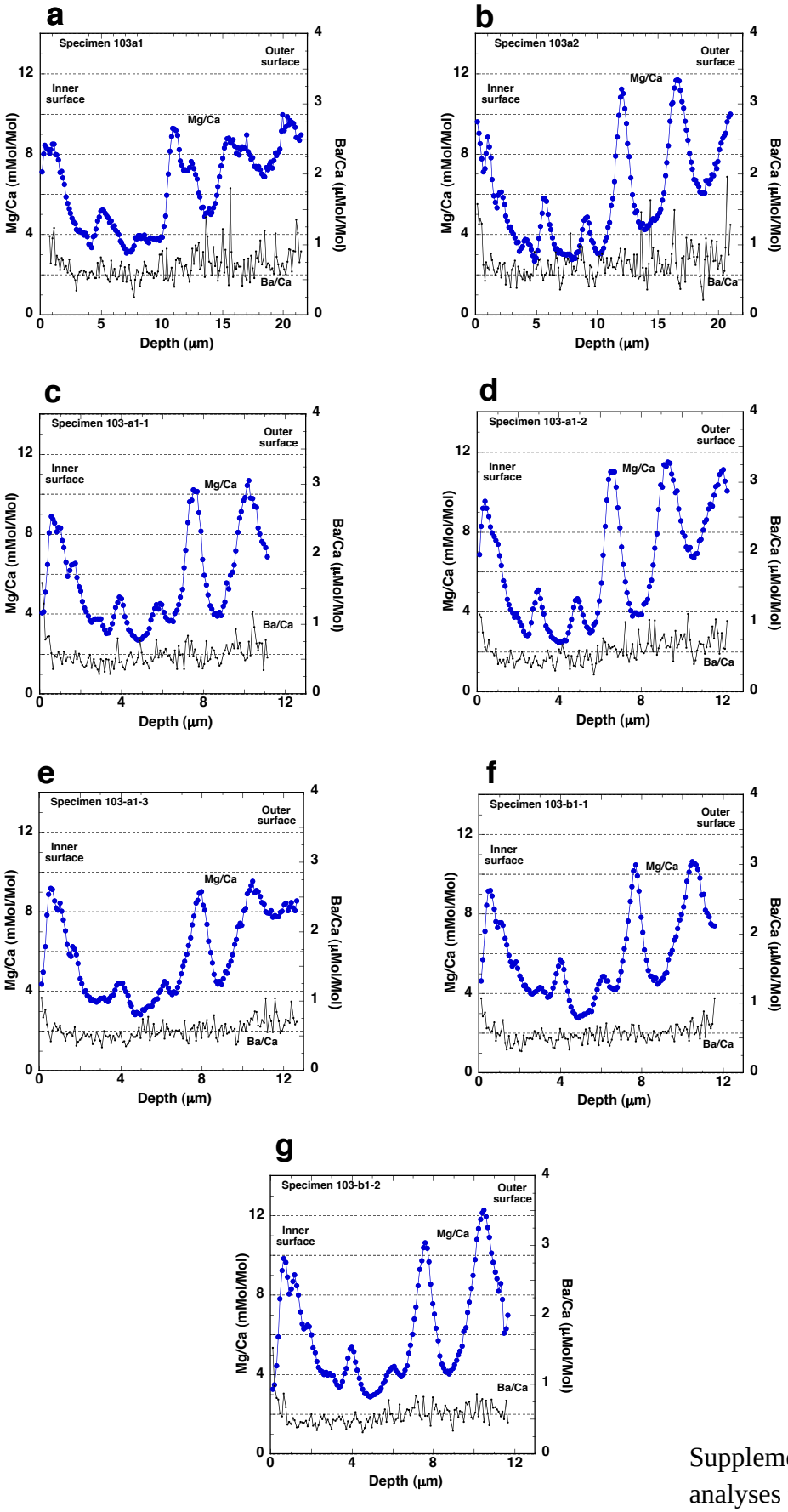

Supplemental Fig. 1: Repeat analyses through specimen 103

Supplemental Table 1: Data from laser ablation profiles of cultured specimens

Sample*	Experiment***	Temp °C	Min Mg/Ca mmol/mol	Max Mg/Ca mmol/mol	Mean Mg/Ca mmol/mol	Mg/Ca ±2 std.err.	Mean Ba/Ca μmol/mol
Group Amb20							
30a1	24h Amb	20	2.1	14.3	6.6		1.18
30a2	24h Amb	20	2.3	12.6	6.1		1.02
51a1	24h Amb	20	5.4	11.7	8.1		0.82
51a2	24h Amb	20	5.1	13.0	8.3		0.77
**103 Avg	24h Amb	20	2.8	10.9	6.0		0.60
Cat2a1	24h Amb	20	2.7	10.7	5.6		0.59
Cat2a2	24h Amb	20	2.8	10.6	5.9		0.56
Average – 24h Amb			***3.4***	***12.2***	***6.8***		***0.82***
Group BD20							
285a	Amb + 12h BaD	20	3.9	6.4	5.4	0.08	
450a1	Amb + 12h BaD	20	2.5	7.5	4.4	0.08	
450a2	Amb + 12h BaD	20	2.0	7.9	4.3	0.10	
451a1	Amb + 12h BaD	20	2.6	8.6	5.4	0.08	
451a2	Amb + 12h BaD	20	3.1	7.4	5.6	0.07	
452a1	Amb + 12h BaD	20	2.0	14.5	5.8	0.24	
452a2	Amb + 12h BaD	20	2.1	13.2	5.6	0.23	
453a1	Amb + 12h BaD	20	2.5	5.8	4.0	0.06	
453a2	Amb + 12h BaD	20	2.8	6.0	4.2	0.06	
463a1	Amb + 12h BaD	20	3.5	14.8	7.1	0.21	
463a2	Amb + 12h BaD	20	3.1	12.3	6.7	0.18	
Average - Amb + 12h BaD			***2.7***	***9.5***	***5.3***	***0.13***	
Group BN20							
#342 Avg	Amb + 12h BaN	20	4.3	9.3	6.4	0.12	
#344 Avg	Amb + 12h BaN	20	3.4	11.2	6.6	0.20	
454a1	Amb + 12h BaN	20	2.7	10.0	5.7	0.15	
454a2	Amb + 12h BaN	20	2.9	11.1	6.3	0.16	
455a1	Amb + 12h BaN	20	2.6	14.9	6.5	0.20	
455a2	Amb + 12h BaN	20	2.7	15.4	6.2	0.19	
457a1	Amb + 12h BaN	20	1.8	4.9	3.0	0.05	
457a2	Amb + 12h BaN	20	1.7	4.5	3.0	0.06	
459a1	Amb + 12h BaN	20	2.4	11.2	6.7	0.16	
459a2	Amb + 12h BaN	20	2.2	12.8	6.3	0.17	
462a1	Amb + 12h BaN	20	2.6	7.1	4.5	0.13	
462a2	Amb + 12h BaN	20	2.3	7.8	4.4	0.17	
501a1	Amb + 12h BaN	20	2.6	7.3	3.9	0.12	
501a2	Amb + 12h BaN	20	2.4	6.7	3.8	0.11	
Average - Amb + 12h BaN			***2.4***	***9.5***	***5.0***	***0.14***	
Group BC20							
533a1	Amb + 24h Ba	20	1.9	10.5	5.9	0.18	1.32
533a2	Amb + 24h Ba	20	2.4	9.1	5.4	0.16	1.01
553a1	Amb + 24h Ba	20	3.0	12.0	6.9	0.16	2.63
553a2	Amb + 24h Ba	20	3.3	12.3	7.1	0.19	2.3
563a1	Amb + 24h Ba	20	4.6	11.8	8.1	0.20	3.62
563a2	Amb + 24h Ba	20	4.6	11.7	8.2	0.23	3.45
563a3	Amb + 24h Ba	20	4.9	10.7	7.7	0.18	3.23
654a1	Amb + 24h Ba	20	3.4	10.7	7.2	0.14	3.72
654a2	Amb + 24h Ba	20	3.0	11.4	7.0	0.19	3.98
Average - Amb + 24h Ba			***3.5***	***11.1***	***7.1***	***0.18***	***2.81***
Group BD25							
464a1	Amb + 12h BaD	25	4.0	13.7	9.7	0.17	
464a2	Amb + 12h BaD	25	3.8	15.7	10.4	0.20	
465a1	Amb + 12h BaD	25	3.9	7.3	4.9	0.11	

465a2	Amb + 12h BaD	25	3.3	8.2	5.0	0.12	
466a1	Amb + 12h BaD	25	9.7	19.4	14.6	0.16	
466a2	Amb + 12h BaD	25	9.5	23.9	15.3	0.23	
470a1	Amb + 12h BaD	25	5.3	12.1	8.0	0.11	
470a2	Amb + 12h BaD	25	4.9	13.8	7.9	0.17	
472a1	Amb + 12h BaD	25	5.6	12.0	8.4	0.16	
472a2	Amb + 12h BaD	25	6.4	9.7	7.6	0.11	
476a1	Amb + 12h BaD	25	6.6	12.2	8.9	0.13	
476a2	Amb + 12h BaD	25	6.3	11.5	9.2	0.10	
Average - Amb + 12h BaD			***5.7***	***13.3***	***9.2***	***0.15***	
Group BN25							
468a1	Amb + 12h BaN	25	6.9	13.7	9.8	0.11	
468a2	Amb + 12h BaN	25	6.9	14.8	10.0	0.12	
471a1	Amb + 12h BaN	25	5.8	12.9	9.6	0.12	
471a2	Amb + 12h BaN	25	5.8	11.6	9.6	0.11	
473a1	Amb + 12h BaN	25	6.4	8.9	7.7	0.06	
473a2	Amb + 12h BaN	25	6.7	9.7	8.1	0.05	
475a1	Amb + 12h BaN	25	3.2	9.4	5.9	0.10	
475a2	Amb + 12h BaN	25	4.0	8.6	5.9	0.08	
477a1	Amb + 12h BaN	25	5.3	12.4	9.0	0.17	
477a2	Amb + 12h BaN	25	5.1	11.1	8.7	0.17	
478a1	Amb + 12h BaN	25	5.5	14.3	10.3	0.17	
478a2	Amb + 12h BaN	25	5.6	14.5	10.2	0.18	
Average - Amb + 12h BaN			***5.6***	***11.8***	***8.7***	***0.12***	
Group BC25							
467a1	Amb + 24h Ba	25	5.6	11.9	8.8	0.11	3.33
467a2	Amb + 24h Ba	25	5.1	12.8	8.7	0.12	3.32
469a1	Amb + 24h Ba	25	2.5	7.0	4.3	0.14	1.09
469a2	Amb + 24h Ba	25	2.5	6.6	4.5	0.14	1.33
579a1	Amb + 24h Ba	25	5.9	13.6	9.4	0.18	4.25
579a2	Amb + 24h Ba	25	4.9	15.0	9.1	0.22	3.79
625a1	Amb + 24h Ba	25	5.4	12.6	8.1	0.20	5.02
625a2	Amb + 24h Ba	25	6.1	12.1	8.6	0.19	4.29
625a3	Amb + 24h Ba	25	6.1	12.0	8.8	0.20	4.39
639a1	Amb + 24h Ba	25	6.3	16.3	9.9	0.23	2.76
639a2	Amb + 24h Ba	25	7.1	14.7	9.4	0.16	2.70
640a1	Amb + 24h Ba	25	9.4	17.2	12.1	0.20	3.36
640a2	Amb + 24h Ba	25	8.8	17.3	12.6	0.24	2.97
640a3	Amb + 24h Ba	25	9.6	15.5	12.1	0.15	2.70
Average - Amb + 24h Ba			***6.1***	***13.2***	***9.0***	***0.18***	***3.24***
Group C3D20							
564a1	Hi CO_3^{2-} + 12hD	20	2.4	6.6	4.3	0.09	
564a2	Hi CO_3^{2-} + 12hD	20	2.2	7.3	4.0	0.09	
608a1	Hi CO_3^{2-} + 12hD	20	3.0	7.7	5.3	0.09	
608a2	Hi CO_3^{2-} + 12hD	20	2.1	9.1	5.2	0.13	
610a1	Hi CO_3^{2-} + 12hD	20	2.1	9.4	4.5	0.10	
610a2	Hi CO_3^{2-} + 12hD	20	2.0	9.3	4.5	0.10	
634a1	Hi CO_3^{2-} + 12hD	20	2.7	11.9	8.3	0.19	
634a2	Hi CO_3^{2-} + 12hD	20	3.4	12.3	8.4	0.18	
647a1	Hi CO_3^{2-} + 12hD	20	1.5	6.6	3.2	0.09	
647a2	Hi CO_3^{2-} + 12hD	20	1.7	7.1	3.3	0.07	
653a1	Hi CO_3^{2-} + 12hD	20	1.8	5.7	3.3	0.06	
653a2	Hi CO_3^{2-} + 12hD	20	2.0	5.7	3.5	0.04	
Average - Hi CO_3^{2-} + 12hD			***2.2***	***8.2***	***4.8***	***0.10***	
Group C3N20							
527a1	Hi CO_3^{2-} + 12hN	20	1.8	10.9	6.7	0.16	
527a2	Hi CO_3^{2-} + 12hN	20	1.6	11.0	6.5	0.17	
528a1	Hi CO_3^{2-} + 12hN	20	2.9	7.0	5.0	0.09	

528a2	Hi CO_3^{2-} + 12hN	20	3.0	6.9	5.0	0.08	
568a1	Hi CO_3^{2-} + 12hN	20	5.4	8.4	6.9	0.06	
568a2	Hi CO_3^{2-} + 12hN	20	5.4	7.9	6.8	0.04	
604a1	Hi CO_3^{2-} + 12hN	20	3.0	7.2	5.2	0.06	
604a2	Hi CO_3^{2-} + 12hN	20	3.4	6.9	5.0	0.05	
605a1	Hi CO_3^{2-} + 12hN	20	2.9	6.4	4.4	0.07	
605a2	Hi CO_3^{2-} + 12hN	20	2.9	6.8	4.8	0.09	
605a3	Hi CO_3^{2-} + 12hN	20	3.6	6.6	4.9	0.07	
609a1	Hi CO_3^{2-} + 12hN	20	2.8	13.7	5.4	0.10	
609a2	Hi CO_3^{2-} + 12hN	20	3.4	8.8	5.7	0.06	
Average - Hi CO_3^{2-} + 12hN			***3.2***	***8.4***	***5.6***	***0.08***	
Group C3C20							
591a1	Hi CO_3^{2-} + 24h	20	2.3	3.3	3.0	0.15	2.2
591a2	Hi CO_3^{2-} + 24h	20	1.8	3.4	2.4	0.08	2.1
593a1	Hi CO_3^{2-} + 24h	20	3.0	9.3	5.2	0.11	2.3
593a2	Hi CO_3^{2-} + 24h	20	3.1	9.8	5.4	0.12	2.4
626a1	Hi CO_3^{2-} + 24h	20	1.5	9.3	4.7	0.11	2.2
626a2	Hi CO_3^{2-} + 24h	20	1.6	9.3	4.6	0.10	2.1
635a1	Hi CO_3^{2-} + 24h	20	1.3	7.3	3.7		2.4
635a2	Hi CO_3^{2-} + 24h	20	1.4	7.5	3.6		2.9
655a1	Hi CO_3^{2-} + 24h	20	1.8	7.7	4.2	0.12	2.2
655a2	Hi CO_3^{2-} + 24h	20	1.5	7.0	3.6	0.12	2.5
Average - Hi CO_3^{2-} + 24h			***1.9***	***7.4***	***4.0***	***0.11***	***2.3***
Group C3D25							
546a1	Hi CO_3^{2-} + 12hD	25	3.4	15.4	8.9	0.25	
546a2	Hi CO_3^{2-} + 12hD	25	6.0	12.8	9.3	0.12	
547a1	Hi CO_3^{2-} + 12hD	25	4.7	14.1	8.6	0.20	
547a2	Hi CO_3^{2-} + 12hD	25	5.0	12.8	8.3	0.17	
548a1	Hi CO_3^{2-} + 12hD	25	3.1	17.9	6.6	0.22	
548a2	Hi CO_3^{2-} + 12hD	25	2.8	10.4	5.8	0.17	
559a1	Hi CO_3^{2-} + 12hD	25	1.8	10.8	4.6	0.13	
559a2	Hi CO_3^{2-} + 12hD	25	2.2	9.1	4.5	0.11	
578a1	Hi CO_3^{2-} + 12hD	25	7.3	15.1	10.6	0.14	
578a2	Hi CO_3^{2-} + 12hD	25	7.7	15.6	10.9	0.15	
Average - Hi CO_3^{2-} + 12hD			***4.4***	***13.4***	***7.8***	***0.17***	
Group C3N25							
520a1	Hi CO_3^{2-} + 12hN	25	5.0	13.3	9.4	0.17	
520a2	Hi CO_3^{2-} + 12hN	25	4.9	15.5	9.7	0.18	
600a1	Hi CO_3^{2-} + 12hN	25	5.3	14.1	9.1	0.15	
600a2	Hi CO_3^{2-} + 12hN	25	5.3	14.6	9.3	0.17	
602a1	Hi CO_3^{2-} + 12hN	25	5.2	9.1	7.2	0.06	
602a2	Hi CO_3^{2-} + 12hN	25	5.1	9.2	7.2	0.06	
603a1	Hi CO_3^{2-} + 12hN	25	3.2	11.4	7.4	0.17	
603a2	Hi CO_3^{2-} + 12hN	25	3.8	11.2	7.1	0.15	
668a1	Hi CO_3^{2-} + 12hN	25	4.2	12.1	7.7	0.16	
668a2	Hi CO_3^{2-} + 12hN	25	4.6	12.3	8.0	0.16	
669a1	Hi CO_3^{2-} + 12hN	25	6.2	16.8	11.4	0.20	
669a2	Hi CO_3^{2-} + 12hN	25	6.8	14.6	10.6	0.18	
Average - Hi CO_3^{2-} + 12hN			***5.0***	***12.9***	***8.7***	***0.15***	
Group C3C25							
529a1	Hi CO_3^{2-} + 24h	25	4.7	13.3	8.7	0.16	4.0
529a2	Hi CO_3^{2-} + 24h	25	4.1	14.5	8.2	0.18	4.0
530a1	Hi CO_3^{2-} + 24h	25	5.3	11.0	7.9	0.08	3.6
530a2	Hi CO_3^{2-} + 24h	25	5.5	11.2	8.0	0.08	3.6
542a1	Hi CO_3^{2-} + 24h	25	4.6	[t]32.9	[t]16.1	0.45	4.5
542a2	Hi CO_3^{2-} + 24h	25	7.7	[t]38.4	[t]17.5	0.44	4.7
543a1	Hi CO_3^{2-} + 24h	25	5.4	11.7	8.0	0.12	2.8
543a2	Hi CO_3^{2-} + 24h	25	6.0	11.4	8.0	0.10	2.4

545a1	Hi CO_3^{2-} + 24h	25	6.3	15.9	11.0	0.15	2.3
545a2	Hi CO_3^{2-} + 24h	25	7.4	15.5	11.2	0.12	2.4
594a1	Hi CO_3^{2-} + 24h	25	2.8	7.8	5.1	0.07	2.7
594a2	Hi CO_3^{2-} + 24h	25	2.6	8.1	5.2	0.09	2.4
Average - Hi CO_3^{2-} + 24h			***5.2***	***12.0***	***8.1***	***0.17***	***3.3***

*'a' denotes the specific test fragment profiled; suffix denotes ablation hole (e.g. a2 = 1st fragment, 2nd hole)

**Data correspond to plots in Fig. A1.

***Amb = ambient sw ([CO_3^{2-}] = 171 μmol kg^{-1}); Hi CO_3^{2-} = 343 μmol kg^{-1}); Ba/Ca data only from 12h:12h L:D (Amb) or 24h Ba-spike experiments

[#]Specimens 342 and 344 did not initiate sphere formation in the laboratory; they were collected with ~one-day-old spherical chambers.

[t]Not included in average.